Available online at www.sciencedirect.com
ScienceDirect
Journal of the European Ceramic Society 28 (2008) 1995–2002
www.elsevier.com/locate/jeurceramsoc

Sintering of tricalcium phosphate–fluorapatite composites with zirconia

Foued Ben Ayed*, Jamel Bouaziz

Laboratory of Industrial Chemistry, National School of Engineering, BP W, 3038 Sfax, Tunisia

Received 2 November 2007; received in revised form 5 February 2008; accepted 8 February 2008
Available online 1 April 2008

Abstract

Zirconia (ZrO_2) addition effects on densification and microstructure of tricalcium phosphate–26.52 wt% fluorapatite composites were investigated, using X-ray diffraction, scanning electron microscopy and by analysis using ^{31}P nuclear magnetic resonance. The tricalcium phosphate–26.52 wt% fluorapatite–zirconia composites densification increases versus temperature. At 1300 °C, the composites apparent porosity reaches 9% with 5 wt% zirconia. XRD analysis of the composites reveals the presence of tricalcium phosphate, fluorapatite and zirconia without any other structures. Above 1300 °C, the densification was hindered by grain growth and the formation of both intragranular porosity and new compounds. The ^{31}P MAS-NMR analysis of composites sintered at various temperatures or with different percentages of zirconia reveals the presence of tetrahedral P sites. At 1400 °C, XRD analysis of the tricalcium phosphate–26.52 wt% fluorapatite–20 wt% zirconia composites shows the presence of calcium zirconate and tetracalcium phosphate. This result indicated that partial decomposition of tricalcium phosphate during sintering process of composites when 20 wt% or less ZrO_2 was added. Thus, zirconia reacts with tricalcium phosphate forming calcium zirconate and tetracalcium phosphate.

Keywords: Sintering; Composites; Porosity; Microstructure-final; Chemical properties; Fluorapatite; ZrO_2; Biomedical applications

1. Introduction

The biocompatibility of biomaterials has been an important concern in many load-bearing biomedical applications.[1,2] Bioceramics have been introduced in the biomaterial industry as a solution to this dilemma.[3,4] Calcium phosphates based materials have attracted considerable interest for orthopaedic and dental applications.[1–16] These biomaterials belong to an important family of bioceramics resembling the part of calcified tissues, particularly hydroxyapatite (Hap), tricalcium phosphate (TCP) and fluorapatite (Fap).

Among these calcium phosphates, tricalcium phosphate (β-TCP) has received recognition in this field.[5–10] β-TCP has gained much attention during the past decade in the applications of orthopaedics' and dentistry.[5–8] The β-TCP has been used clinically to repair bone defects for many years.[8,9] Especially Fap among these materials has excellent biocompatibility with the adjacent hard tissue.[8,11–16] The Fap is known to have a high chemical stability of Hap.[8,11–18] At 1250 °C, Hap decomposes to TCP,[17] whereas Fap remains stable.[12,14] Moreover, Fap has a potential advantage by comparison with Hap grace its higher thermal stability and aptitude to delay caries process without the biocompatibility degradation.[8,12,14,15] In this study, Fap has been used with a fixed 26.52 wt% amount because the human bone contains 1 wt% of fluorine, approximately.[33]

However, mechanical properties of calcium phosphates are generally inadequate for many load-carrying applications. These bioceramics have a low density decreasing the mechanical properties.[6–8,11,15,17] Hence, bioinert ceramic oxides like alumina (Al_2O_3) and zirconia (ZrO_2) having high strength is used to enhance the densification and the mechanical properties of bioceramic.[18–33] However, there is serious problem in incorporating the zirconia with the Hap at low temperature (at 1150 °C); reaction between the ZrO_2 and Hap.[20,21,23–32] These reactions not only reduce the mechanical properties but also degrade the biocompatibility of the bioceramic.[23–29] For this reason, zirconia was chosen as a framework for load-bearing and TCP and Fap were chosen as an outer coating to enhance the biocompatibility and osteoconductivity. Therefore, because of its high mechanical strength, toughness, and inertness in the human body, zirconia improves the properties of TCP and as a second phase. This article propose to study the sintering of TCP–26.52 wt% Fap composites at various temperatures (1100 °C, 1200 °C, 1300 °C and 1400 °C) and with different percentages of zirco-

* Corresponding author. Tel.: +216 98 252 033; fax: +216 74 275 595.
E-mail address: benayedfoued@yahoo.fr (F. Ben Ayed).

0955-2219/$ – see front matter © 2008 Elsevier Ltd. All rights reserved.
doi:10.1016/j.jeurceramsoc.2008.02.004

Table 1
Characteristics of the powders used in the study

Compounds	SSA (m^2/g) ±1.0	D_{BET} (μm) ±0.2	D_{50} (μm)[a] ±0.2	DTA measurements (endothermic peak)	T (°C)[b]	TEC[c] ($\times 10^{-6}$ °C^{-1})	d[d]
Fap [12]	29.00	0.07	6	1180 °C (liquid phase)	715	7.4–11.9[34]	3.19
TCP [10]	1.13	1.73	9	1285 °C (β → α) 1475 °C (α → α′)	1050	12[35]	3.07 (β) 2.86 (α)
Composite [16] [e]	1.20	1.60	11	–	1080	–	3.10
Zirconia	2.01	0.50	5	–	1110	12–14[36]	5.83 (m)[f]

[a] Mean diameter.
[b] Sintering temperature.
[c] Thermal Expansion Coefficient.
[d] Theoretical density.
[e] TCP–26.52% Fap.
[f] Monoclinic.

nia (2.5 wt%; 5 wt%; 10 wt% and 20 wt%) and to characterize the resulting composites with density, X-ray diffraction, nuclear magnetic resonance (^{31}P) and scanning electron microscopy measurements.

2. Experimental methods

2.1. Preparation of powder and ceramic specimens

Fap powder is synthesized by precipitation method.[12] Analytical grade $Ca(NO_3)_2{\cdot}4H_2O$ (Merck), $(NH_4)_2HPO_4$ (Merck), and NH_4F (Merck), were used as the starting materials. A solution of 0.3 mol $Ca(NO_3)_2$ in 750 ml distilled water was poured using a peristaltic pump into a boiling solution of 0.18 mol $(NH_4)_2HPO_4$ and 0.12 mol NH_4F in 750 ml distilled water; 28% NH_4OH (Merck) solution was added to the mixture and the pH was adjusted to 9. The precipitate was aged with stirring at 80 °C for 3 h, then filtered, washed, dried at 70 °C for 12 h and calcined at 500 °C.

The β-TCP powder was synthesized by solid-state reaction.[23] A calcium carbonate ($CaCO_3$, Merck) was added to diammonium hydrogenophosphate ($(NH_4)_2HPO_4$, Merck) at 900 °C, according to the following reaction:

$$3CaCO_3 + 2(NH_4)_2HPO_4 \rightarrow \beta\text{-}Ca_3(PO_4)_2 + 3CO_2 + 4NH_3 + 3H_2O \quad (1)$$

Monoclinic zirconia (m-ZrO_2) powder (Merck) was used in all experiments. Characteristics experiments of zirconia powder are illustrated in Table 1.

The β-TCP, Fap and zirconia powder are mixed in an agate mortar. The powder mixtures were milled in ethanol for 24 h. After milling, the mixtures were dried in a rotary vacuum evaporator and passed through a 70-mesh screen. After drying at 80 °C for 24 h, the powder mixtures are moulded in a cylinder having a 13-mm diameter and 4-mm thickness and pressed under 150 MPa. The green compacts are sintered at various temperatures (1100 °C, 1200 °C, 1300 °C and 1400 °C) during 1 h. The green compacts are sintered in a vertical furnace (Pyrox 2408). The best hold time for obtaining the maximum densification is 1 h. The heating rate is 10 °C min^{-1}. The bulk density of the sintered body was calculated from the dimensions and weight (geometrical measurement). The relative error of apparent porosity value was about 1%.

The calculated theoretical densities of each composite and the weight rates of each used compounds were illustrated in Table 2. The theoretical density (d) was determined using the following equation:

$$d = \frac{3.07A + 3.19B + 5.83C}{100} \quad (2)$$

where A, B, C are the weight rates and 3.07, 3.19, 5.83 are the theoretical densities of β-TCP, Fap and zirconia, respectively.

2.2. Characterization methods of powder and ceramic specimens

Linear shrinkage was determined by dilatometry (Setaram TMA 92 dilatometer). The heating and cooling rates were 10 °C min^{-1} and 20 °C min^{-1}, respectively. Powders were previously compacted in a 13-mm cylinder die. The specific surface area (SSA) was measured by the BET method using N_2 as an adsorption gas (ASAP 2010).[37] The primary particle size (D_{BET}) was calculated by assuming the primary particles to be spherical [14]:

$$D_{BET} = \frac{6}{S\rho} \quad (3)$$

where ρ is the theoretical density of compounds and S is the SSA.

The granulometry distribution of powders was analysed by a laser granulometer (Micromeritics Sedigraph 5000). The X-ray

Table 2
Theoretical densities of each composite and the weight rates of each compound used for each composite (A, B and C are the weight rates of β-TCP, Fap and zirconia, respectively)

Composites/weight rates	A (%)	B (%)	C (%)	d[a]
TCP–Fap	73.48	26.52	0	3.101
TCP–Fap–2.5 ZrO_2	70.98	26.52	2.5	3.170
TCP–Fap–5 ZrO_2	68.48	26.52	5	3.240
TCP–Fap–10 ZrO_2	63.48	26.52	10	3.378
TCP–Fap–20 ZrO_2	53.48	26.52	20	3.654

[a] Theoretical density.

diffraction pattern of sintered pieces was performed by a Seifert XRD 3000 TT diffractometer, with monochromatized Cu Kα radiation (at 20 A and 40 kV). The samples were scanned in the diffraction angle range (2θ) varying from 10° to 60° with a step length of 0.02° (2θ) and a counting time of 1 s step^{-1}. The crystalline phases are identified from powder diffraction files (PDFs) of the International Center for Diffraction Data (ICDD). The TCP–Fap composites were characterized by high-resolution solid-state MAS-NMR using a BRUKER 300WB spectrometer. The ^{31}P observational frequency was 121.49 MHz with 3.0 ms pulse duration, spin speed 8000 Hz and delay 1 s with 2048 scans. ^{31}P shift is given in parts per million (ppm) referenced to 85 wt% H_3PO_4. The microstructure of sintered compacts was investigated by scanning electron microscope (Philips XL 30) on fractured sample surfaces. Because calcium phosphates are insulating biomaterial, the sample was coated with gold for more electronic conduction. The grain mean size was measured directly from SEM micrographs.

3. Results and discussion

3.1. Sinterability of TCP–Fap–zirconia composites

Linear shrinkage of β-TCP, Fap, TCP–26.52 wt% Fap composites and zirconia starts at about 1050 °C, 715 °C, 1080 °C and 1110 °C, respectively (Table 1). The addition of 26.52 wt% Fap in the matrix of β-TCP increases the sintering temperature of 30 °C by comparison with the pure β-TCP. The study of zirconia dilatometric behaviour showed that shrinkage began at about 1100 °C, which is superior to these sintering temperatures of TCP and TCP–26.52 wt% Fap composites (Table 1). The thermal expansion coefficient (TEC) of each compound presents practically the same value in literature.[34–36] In fact, the TEC of β-TCP from 50 °C to 400 °C is 12×10^{-6} °C^{-1}.[35] While Fap has TEC values of (7.4–11.9) $\times 10^{-6}$ °C^{-1} (20–300 °C).[34] The TEC of zirconia is similar with β-TCP TEC, It is between 12×10^{-6} °C^{-1} and 14×10^{-6} °C^{-1} [36] (Table 1).

The SSA of β-TCP, Fap, TCP–26.52 wt% Fap composites and zirconia are 1.13 m^2/g, 29.00 m^2/g, 1.20 m^2/g and 2.01 m^2/g, respectively. The Fap and β-TCP particles are assumed to be spherical; the particle size can be calculated using Eq. (3). The results of average grain size obtained by SSA (D_{BET}) and average grain size obtained by granulometric repartition (D_{50}) are presented in Table 1. These values (D_{BET}) obtained by SSA do not correspond to those obtained from the particle size distribution (Table 1). The discrepancy may be due to the presence of agglomerates which are formed during preparations of β-TCP powder at 900 °C and calcinations of Fap powder at 500 °C.

Fig. 1 shows the XRD patterns of the β-TCP powder synthesized at 900 °C (Fig. 1a) and β-TCP powder calcined at various temperatures (1240 °C and 1300 °C) (Fig. 1b and c). These samples reveal only peaks of β-TCP (ICDD data file no. 9-169). Calcination of the powders at 1300 °C indicates the improvement in crystallinity by the increase in the resolution of peaks when compared to the as-prepared powder. Fig. 2 presents the XRD patterns of Fap powder calcined at varying temperatures. At 900 °C, the XRD pattern of Fap powder shows the presence

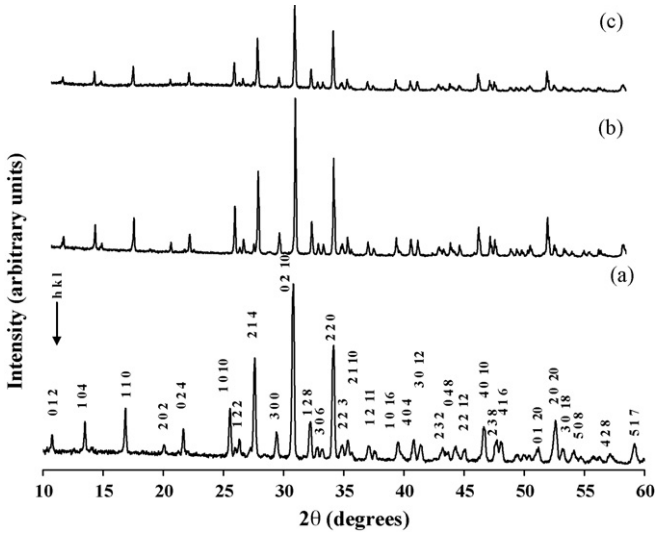

Fig. 1. XRD patterns for β-TCP: (a) synthesized powder at 900 °C; (b) calcined powder at 1240 °C; (c) calcined powder at 1300 °C.

of calcium fluoride traces (CaF_2) (ICDD data file no. 65-0535) in the Fap matrix (ICDD data file no. 15-876) (Fig. 2a). When the temperature increased to 1300 °C, the intensity of calcium fluoride characterized peak gradually decreased and a small amount of CaO is observed (ICDD data file no. 37-1497) (Fig. 2b). The CaO traces has been detected by XRD and phenolphthalein test in samples. This experiment shows that the formation of CaO during the calcination can only be the result of the hydrolysis of fluorite.[14] CaF_2 is contained in the synthesised Fap powder as impurity. The X-ray diffraction pattern for zirconia powder is presented in Fig. 3. It is well seen from the pattern that only the monoclinic zirconia (m-ZrO_2) phase is detected (ICDD data file no. 37-1484).

The powder's sinterability is examined by firing, between 1100 °C and 1400 °C for 1 h. Fig. 4 shows the typical relationship between sintering temperature and apparent porosity of TCP–26.52 wt% Fap composites sintered for 1 h with different percentages of ZrO_2 (2.5 wt%; 5 wt%; 10 wt% and 20 wt%). The apparent porosity decreases with sintering temperature (Table 3). This curve which illustrates a minimum apparent

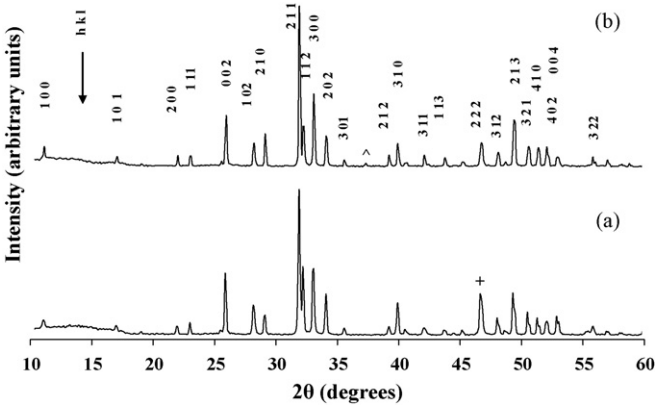

Fig. 2. XRD patterns for Fap powder calcined at: (a) 900 °C and (b) 1300 °C (+: CaF_2 and ^: CaO).

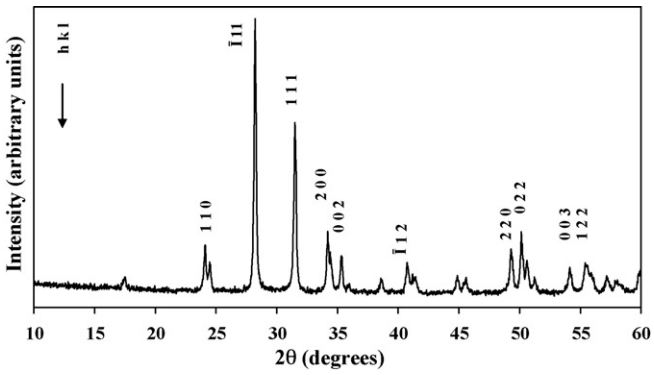

Fig. 3. XRD pattern for monoclinic zirconia powder.

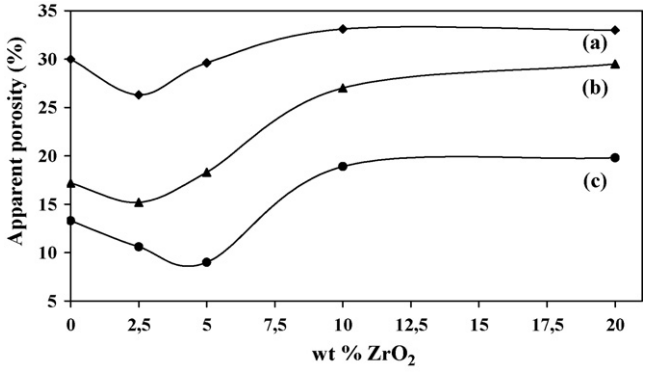

Fig. 4. Apparent porosity versus temperature and mass percentages of zirconia of TCP–26.52 wt% Fap composites sintered for 1 h at: (a) 1100 °C; (b) 1200 °C; (c) 1300 °C.

porosity at about 9% corresponding to the composites sintered with 5 wt% ZrO_2 (Table 3). The porosity of the sintered composites increased with increase of zirconia concentration in the composites. At 1400 °C, their densities are impossible to be determinates because the samples are cooled in the support. With 10 wt% ZrO_2, the composite densification decreases with any sintering temperature.

3.2. Characterization of sintered samples

The evolution of the local environment of the phosphorus atoms was followed during the sintering process by ^{31}P MAS-NMR.

Table 3
Apparent porosity versus temperature of TCP–26.52 wt% Fap composites sintered with different wt% of ZrO_2 for 1 h

wt% ZrO_2/*T* (°C)	Apparent porosity ±1 (%)		
	1100	1200	1300
0	30.0	17.2	13.3
2.5	26.3	15.2	10.6
5	29.6	18.3	9.0
10	33.1	27.0	18.9
20	33.0	29.5	19.8

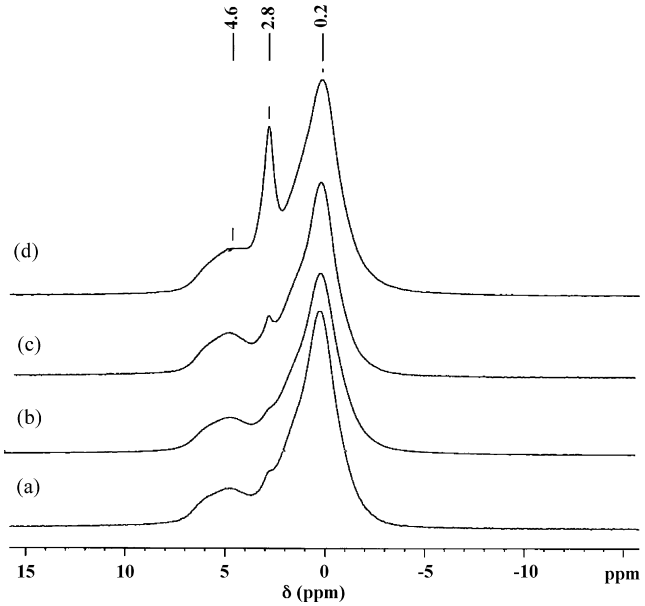

Fig. 5. ^{31}P MAS-NMR spectra of TCP–26.52 wt% Fap composites sintered with 2.5 wt% ZrO_2 for 1 h at: (a) 1100 °C; (b) 1200 °C; (c) 1300 °C; (d) 1400 °C.

The spectra of TCP–26.52 wt% Fap composites content 2.5 wt% zirconia sintered for 1 h at various temperatures (1100 °C, 1200 °C, 1300 °C and 1400 °C) is presented in Fig. 5; which shows a broad peaks (centred on 4.6 ppm) and intense peaks at 0.2 ppm; that is assigned to the phosphorus tetrahedral P sites relative of TCP. The same figure illustrates an intense peak at 2.8 ppm relative, to the phosphorus of Fap, can be assigned to tetrahedral sites (Q^1). The ^{31}P MAS-NMR spectra of TCP illustrate three peaks (at 4.60 ppm, 0.20 ppm and 1.02 ppm) (Fig. 5a). The same result was found by Yashima et al. [38] Indeed, they show that the phosphorus atoms are located in three crystallographic sites of $P(1)O_4$, $P(2)O_4$ and $P(3)O_4$. In the ^{31}P MAS-NMR spectra of the composite, the peak relative to Fap increases with sintering temperatures (Fig. 5c and d) (1300–1400 °C). This can be attributed to the solid reaction between CaF_2 and TCP. CaF_2 is assumed to be formed as a second phase during the Fap powder preparation.[12] However, the Fap DTA curve shows an endothermic peak at 1180 °C relative to an eutectic formed between Fap and CaF_2 (Table 1).[12] The solid reaction of the new quantity of Fap is the following [16,33]:

$$3Ca_3(PO_4)_{2(s)} + CaF_{2(s)} \rightarrow Ca_{10}(PO_4)_6F_{2(s)} \quad (4)$$

The ^{31}P MAS-NMR spectra of TCP–26.52 wt% Fap composites sintered for 1 h at 1300 °C with different percentages of ZrO_2 (2.5 wt%; 5 wt%; 10 wt% and 20 wt%) reveal the presence of tetrahedral P sites (0.20; 1.19; 2.80 and 4.70 ppm) (Fig. 6).

The ^{31}P MAS-NMR spectra of TCP–26.52 wt% Fap composites sintered for 1 h at 1400 °C with various wt% of ZrO_2 (2.5 wt%; 5 wt%; 10 wt% and 20 wt%) are presented in Fig. 7. These spectra present practically the same structure, which show peaks relative to TCP (0.2 ppm and 4.7 ppm) and Fap (2.8 ppm). Exceptionally, the ^{31}P MAS-NMR spectrum of composites sintered with 20 wt% ZrO_2 illustrates the increase of the peak

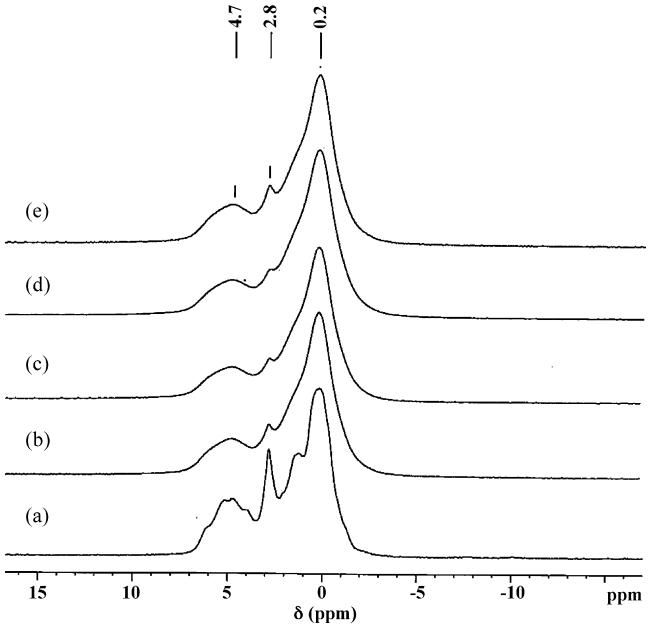

Fig. 6. ^{31}P MAS-NMR spectra of TCP–26.52 wt% Fap composites sintered at 1300 °C for 1 h with different mass percentages of ZrO_2: (a) 0 wt%; (b) 2.5 wt%; (c) 5 wt%; (d) 10 wt%; (e) 20 wt%.

intensity relative to Fap for the samples. However, when the sintering temperature increases to 1400 °C (Fig. 7d), the TCP peak relativity decreases, illustrating probably a pronounced partials decomposition of TCP.

The X-ray diffraction patterns of TCP–26.52 wt% Fap composites heated at various temperatures for 1 h with 2.5 wt% ZrO_2 are reported in Fig. 8. The XRD patterns of samples sintered

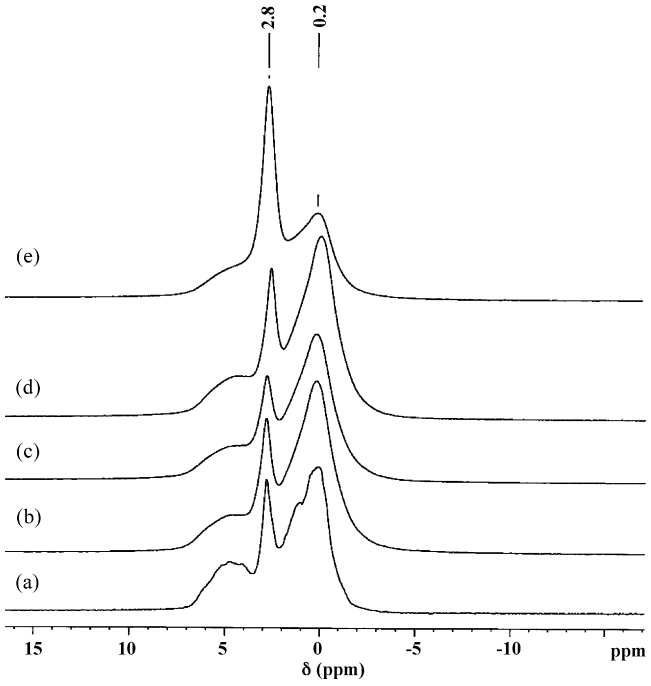

Fig. 7. ^{31}P MAS-NMR spectra of TCP–26.52 wt% Fap composites sintered at 1400 °C for 1 h with different mass percentages of ZrO_2: (a) 0 wt%; (b) 2.5 wt%; (c) 5 wt%; (d) 10 wt%; (e) 20 wt%.

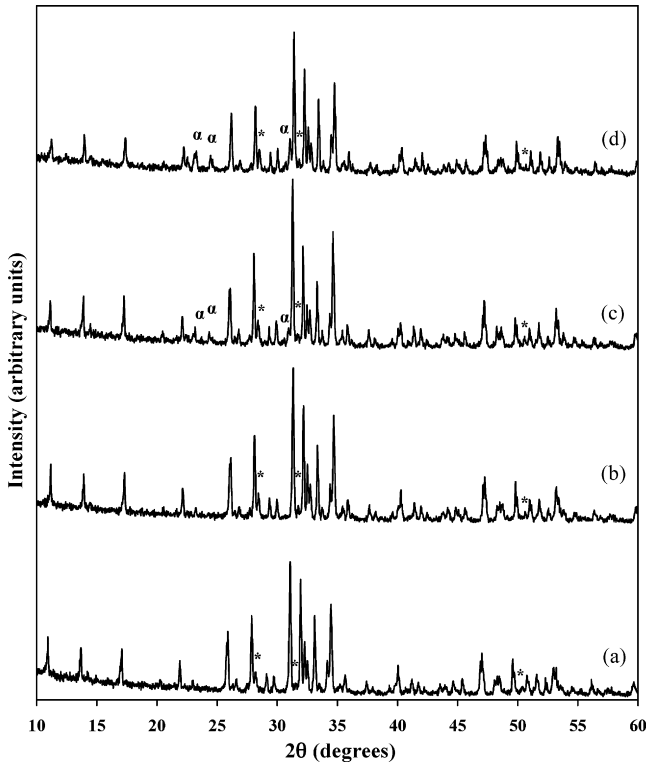

Fig. 8. XRD patterns of TCP–26.52 wt% Fap composites sintered with 2.5 wt% ZrO_2 for 1 h at: (a) 1100 °C; (b) 1200 °C; (c) 1300 °C; (d) 1400 °C (α: α-TCP and *: m-ZrO_2).

at various temperatures (1100–1400 °C), show the presence of β-TCP; Fap and m-ZrO_2 traces. When sintered at 1100 °C (Fig. 8a), the composites retained the initial phases (β-TCP and Fap). In the composite fabricated at 1200 °C, the resulting phases were similar to that case at 1100 °C. However, when the sintering temperature increases to 1300 °C (Fig. 8c and d), X-ray diffraction patterns show also the presence of α-TCP traces (ICDD data file no. 9-348). The highest (2θ) peak positions of α-TCP are placed at 30.75°, 24.09° and 22.90°.

The XRD analysis of TCP–26.52 wt% Fap composites sintered at 1400 °C for 1 h with various zirconia additives amounts (0 wt%; 2.5 wt% and 20 wt%) is presented in Fig. 9. The TCP–26.52 wt% Fap composites sintered without and with zirconia (2.5 wt%) contained initial phases (β-TCP, Fap and α-TCP traces) (Fig. 9a and b). The effect of zirconia during sintering process was observed in XRD pattern in Fig. 9c. The sample sintered with 20 wt% ZrO_2 shows the presence of calcium zirconate ($CaZrO_3$: CZ), Fap, tetracalcium phosphate ($Ca_4(PO_4)_2O$: TTCP (ICDD data file no. 5-1137)), m-ZrO_2 traces, tetragonal-zirconia traces (t-ZrO_2: ICDD data file no. 17-0923), α-TCP traces, and β-TCP traces (Fig. 9c).

At 1400 °C, when the TCP–26.52 wt% Fap composites was sintered with zirconia (less than 20 wt%), CZ and TTCP peaks were observed by XRD, which suggests partial decomposition on TCP to CZ. This result is confirmed by ^{31}P MAS-NMR analysis (Fig. 7e). The presence of CZ and TTCP is observed by Khor et al.[20] and Heimann and Vu.[30] They have shown that addition of CaO to Hap–ZrO_2 composite mixtures shifts the chemical

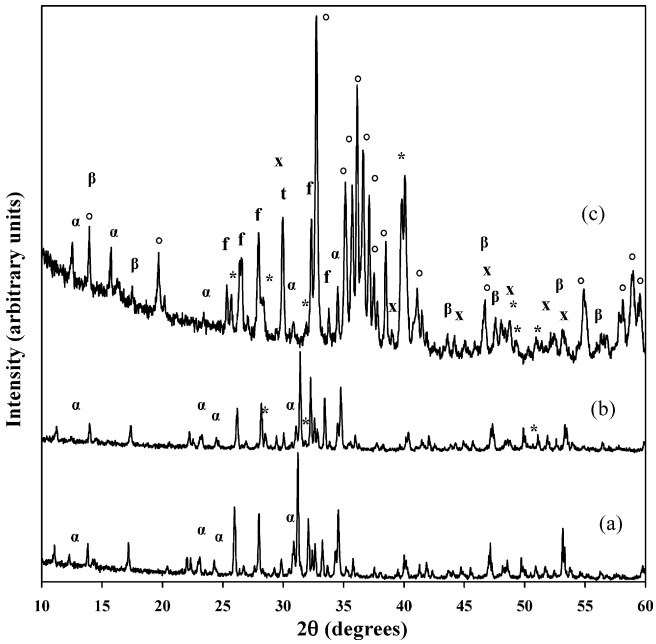

Fig. 9. XRD patterns of TCP–26.52 wt% Fap–zirconia composites sintered for 1 h at 1400 °C with: (a) 0 wt% ZrO_2; (b) 2.5 wt% ZrO_2; (c) 20 wt% ZrO_2; (α: α-TCP; β: β-TCP; *: ZrO_2; °: CZ; x: TTCP; f: Fap; t: t-ZrO_2).

equilibrium of the product from TCP and TTCP towards Hap making it more stable.[30] Surplus CaO will be effectively fixed by ZrO_2 acting as a sink for Ca^{2+} ions resulting in the formation of either tetragonal zirconia (t-ZrO_2) or CZ.[30]

Moreover, the CZ was also produced, suggesting the diffusion of calcium in zirconia during the sintering process of the TCP–26.52 wt% Fap–20 wt% ZrO_2 composites. The partial decomposition of TCP with zirconia at 1400 °C can be described by the following reactions:

$$Ca_3(PO_4)_{2(s)} + \text{m-}ZrO_{2(s)} + 2CaO_{(s)} \leftrightarrow Ca_4(PO_4)_2O_{(s)} + CaZrO_{3(s)} \quad (5)$$

$$ZrO_{2(s)} + CaO_{(s)} \leftrightarrow CaZrO_{3(s)} \quad (6)$$

CaO is produced by solid reaction between CaF_2 and H_2O.[12,14,15] Fluorite (CaF_2) is assumed to be formed as a second phase during the powder preparation of Fap. Ben Ayed et al.[12] show that when the gas atmosphere is not fittingly dried, hydroxyfluorapatite can be formed and hydrolysis of CaF_2, which can be expressed by the following equations [14]:

$$CaF_{2(s)} + H_2O_{(g)} \rightarrow CaO_{(s)} + 2HF_{(g)} \quad (7)$$

$$Ca_{10}(PO_4)_6F_{2(s)} + xH_2O_{(g)} \rightarrow Ca_{10}(PO_4)_6F_{2-x}(OH)_{x(s)} + xHF_{(g)} \quad (8)$$

In TCP–26.52 wt% Fap composites containing 20 wt% ZrO_2 or more, CZ is formed after reaction at 1400 °C. At these conditions, the increased tendency of decomposition of TCP with reaction with ZrO_2 can be explained as resulting from removal of calcium from the TCP and its dissolution into the zirconia. This solid solution of calcium into the zirconia leads to its transformation to the tetragonal phase. This result of reaction in Hap–ZrO_2 composites study was confirmed by Evis.[32] In fact, he shows that, the exchange of Ca^{2+} and ZrO^{2+} ions can occur where the surfaces of ZrO_2 and Hap are in contact, with minimum rearrangement of their structures. Different apatite's can have many substitute ions in their structures without causing change from the apatite structure.[39] The exchange of ZrO^{2+} ions for Ca^{2+} ions in the TCP structure explains the increased tendency of the exchanged TCP to decompose.[32] The large ZrO^{2+} ion introduces strain into the TCP network structure, making the decomposition of Eq. (5) more favourable. Eq. (6) occurs at a lower content of zirconia. Thus, Eq. (5) plays an important role in the reaction during sintering process when more zirconia is added to TCP. This equation indicates that, the calcium ions in the TCP diffused into the m-ZrO_2 to CZ. The subsequent reaction (5) is similar to the previous reported by Khor et al. on the effects of ZrO_2 on the phase compositions plasma sprayed Hap-YSZ composites coatings.[20]

The SEM examination of the fracture surface of the TCP–26.52 wt% Fap composites sintered with different percentages of ZrO_2 at various temperatures is reported in Fig. 10. The fracture surfaces clearly reveal a distinct difference in the sample's microstructure; show that at 1100 °C; the composites sintered with 2.5 wt% ZrO_2 presents an intergranular porosity subsequently by eliminated with the grain growth (Fig. 10a and b). Thus, a slight coarsening accompanies densification at 1300 °C (Fig. 10b). The grains' size about 1 μm at 1100 °C and 5 μm at 1300 °C (Fig. 10a and b). At higher temperature (1400 °C), the TCP–26.52 wt% Fap–2.5 wt% zirconia composites densification is hindered by grain growth and the formation of intergranular porosity. The pore, which are roughly spherical have diameter approximately between 1 μm and 3 μm (Fig. 10c). Ben Ayed et al. also observed the formation of large pores at these temperatures, during the study of pressureless sintering of Fap under oxygen atmosphere.[12] They attributed to the departure of volatile species produced by the hydrolysis of Fap and fluorite. At 1400 °C, the increased porosity in the sintered composites with addition of zirconia probably results by the pores formation and by partially decomposition of the TCP (Eq. (5)).

Fig. 10b and d shows the microstructural developments during the sintering of composites at 1300 °C for 1 h with different percentages of ZrO_2 (2.5 wt% and 10 wt%), observed on fractured surfaces by SEM. In the material firing at 1300 °C with 2.5 wt% zirconia, one notices a partially reduction of the porosity (Fig. 10b). The micrograph relative to composites sintered with 10 wt% ZrO_2 reveals an important intragranular porosity (Fig. 10d). From the energy dispersive X-ray analysis (EDAX) on the SEM of TCP–26.52 wt% Fap composites sintered at 1300 °C in Fig. 10d, it is found that the light phase is ZrO_2, which are segregated at the grain boundaries of grey coloured TCP–Fap matrix phases.

At temperatures inferior at 1300 °C, the composites present a good sinterability with 5 wt% zirconia. The XRD analysis of the composites reveals the initial phases (TCP and Fap). Adolfsson et al.[18] confirm this result during its study on zirconia–Fap materials produced by HIP. In fact, they show that, the Fap

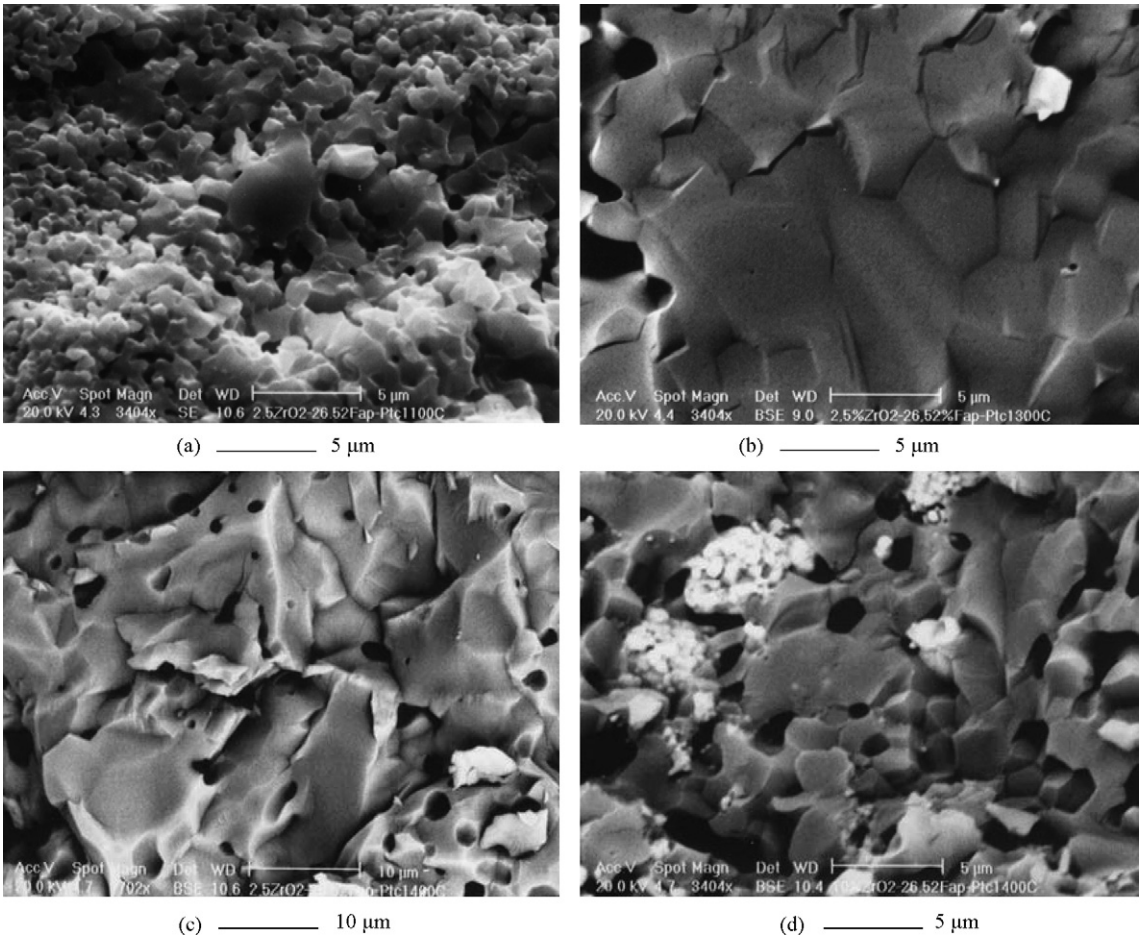

Fig. 10. SEM micrographic of TCP–26.52 wt% Fap composites sintered for 1 h at various temperatures with different percentages of zirconia: (a) 2.5 wt%, 1100 °C; (b) 2.5 wt%, 1300 °C; (c) 2.5 wt%, 1400 °C; (d) 10 wt%, 1300 °C.

remains stable at 1200 °C and without any other structure was observed.[18] These results clearly illustrate the effect of the Fap layer prevented the reaction between TCP and ZrO_2 at temperature less than 1300 °C. Indeed, no chemical reactions are observed among the materials with introducing the Fap at high temperature (1300 °C). At temperatures higher than 1300 °C (1400 °C), the densification of TCP–26.52 wt% Fap–ZrO_2 composites is hindered by grains growth and by the partial decomposition of TCP.

4. Conclusion

The addition of ZrO_2 in the form of particles to calcium phosphate (TCP and Fap) matrix has drawn much attention due to its biocompatibility coupled with the tendency to enhance the mechanical properties of TCP–Fap composites. So, zirconia additive was tested for the TCP–26.52 wt% Fap composites densification. High-density TCP–Fap–ZrO_2 composites were produced after sintering at 1300 °C. A minimal apparent porosity was reached with 5 wt% ZrO_2. In fact, the apparent porosity for the TCP–26.52 wt% Fap–zirconia composites is about 9%. At 1300 °C, XRD analysis of the TCP–26.52 wt% Fap–zirconia composites reveals only the presence of Fap, TCP and zirconia traces. High temperatures (above 1300 °C) or mass percentages of zirconia (near 20 wt%) are not the best conditions for the composites densification. This is probably due to the new compound formation (CZ and TTCP). At 1400 °C, the partial decomposition of TCP during sintering process is increased by addition of zirconia (near 20 wt%). This decomposition involves the exchange of Ca^{2+} and ZrO^{2+} ions between the TCP and zirconia.

References

1. Ducheyne, P. and Healy, K. E., The effect of plasma-sprayed calcium phosphate ceramic coatings on the metal ion release from porous titanium and cobalt–chromium alloys. *J. Biomed. Mater. Res.*, 1988, **22**, 1137–1163.
2. Hemmerle, J., Oncag, A. and Erturk, S., Ultrastructural features of the bone response to a plasma-sprayed hydroxyapatite coating in sheep. *J. Biomed. Mater. Res.*, 1997, **36**, 418–425.
3. Hench, L. L., Splinter, R. J., Allen, W. C. and Greenleen, T. K., Bonding mechanisms at the interface of ceramic prosthetic materials. *J. Biomed. Mater. Res.*, 1972, **2**, 117–141.
4. Doremus, R. H., Bioceramics. *J. Mater. Sci.*, 1992, **27**, 285–297.
5. Hench, L. L., Bioceramics: from concept to clinic. *J. Am. Ceram. Soc.*, 1991, **74**(7), 1487–1510.
6. Mark, F. and Brown, P. W., Low-temperature formation of fluorapatite in aqueous solution. *J. Am. Ceram. Soc.*, 1992, **75**(12), 401–407.

7. Uwe, P., Angela, E. and Christian, R., A pyrolytic route for the formation of Hydroxyapatite-fluorapatite solid solutions. *J. Mater. Sci.: Mater. Med.*, 1993, **4**(3), 292–295.
8. Elliott, J. C., *Structure and Chemistry of the Apatite and Other Calcium Orthophosphates*. Elsevier Science B.V., Amsterdam, 1994.
9. Destainville, A., Champion, E., Bernache-Assolant, D. and Labore, E., Synthesis, characterization and thermal behaviour of apatitic tricalcium phosphate. *Mater. Chem. Phys.*, 2003, **80**, 69–77.
10. Ben Ayed, F., Chaari, K., Bouaziz, J. and Bouzouita, K., Frittage du phosphate tricalcique. *C.R. Phys.*, 2006, **7**(7), 825–835.
11. Franz, E. D. and Telle, R., Reaction hot pressing fluorapatite for dental implants. In *High Tech Ceramics*, ed. P. Vincenzini. Elsevier Science Publishers B. V, Amsterdam, 1987, p. 31.
12. Ben Ayed, F., Bouaziz, J. and Bouzouita, K., Pressureless sintering of fluorapatite under oxygen atmosphere. *J. Eur. Ceram. Soc.*, 2000, **20**(8), 1069–1076.
13. Ben Ayed, F., Bouaziz, J., Khattech, I. and Bouzouita, K., Produit de solubilité apparent de la fluorapatite frittée. *Ann. Chim. Sci. Mater.*, 2001, **26**(6), 75–86.
14. Ben Ayed, F., Bouaziz, J. and Bouzouita, K., Calcination and sintering of fluorapatite under argon atmosphere. *J. Alloys Compd.*, 2001, **322**(1–2), 238–245.
15. Ben Ayed, F., Bouaziz, J. and Bouzouita, K., Résistance mécanique de la fluorapatite frittée. *Ann. Chim. Sci. Mater.*, 2006, **31**(4), 393–406.
16. Ben Ayed, F. and Bouaziz, J., Elaboration et caractérisation d'un biomatériau à base de phosphate de calcium. *C.R. Phys.*, 2007, **8**(1), 101–108.
17. Landi, E., Tampieri, A., Celotti, G. and Sprio, S., Densification behaviour and mechanisms of synthetic hydroxyapatites. *J. Eur. Ceram. Soc.*, 2000, **20**, 2377–2387.
18. Adolfsson, E. and Hermansson, L., Zirconia-fluorapatite materials produced by HIP. *Biomaterials*, 1999, **20**, 1263–1267.
19. Min Kong, Y., Kim, S. and Kim, H. E., Reinforcement of hydroxyapatite bioceramic by addition of ZrO_2 coated with Al_2O_3. *J. Am. Ceram. Soc.*, 1999, **82**(11), 2963–2968.
20. Khor, K. A., Fu, L., Lim, V. J. P. and Cheang, P., The effects of on the phase compositions of plasma sprayed HA/YSZ composite coatings. *J. Mater. Sci. Eng. A*, 2000, **276**, 160–166.
21. Sivakumar, M. and Manjubala, I., Preparation of hydroxyapatite/fluortapatite–zirconia composites using India corals for biomedical applications. *Mater. Lett.*, 2001, **50**, 199–205.
22. Kim, S., Kong, Y. M., Lee, I. S. and Kim, H. E., Effect of calcinations of starting powder on mechanical properties of hydroxyapatite–alumina bioceramic composite. *J. Mater. Sci.: Mater. Med.*, 2002, **13**, 307–310.
23. Ramachandra Rao, R. and Kannan, T. S., Synthesis and sintering of hydroxyapatite–zirconia composites. *J. Mater. Sci. Eng. C*, 2002, **20**, 187–193.
24. Kim, H. W., Lee, Y., Bae, C. J., Nah, Y. J. and Kim, H. E., Reaction sintering and mechanical properties of hydroxyapatite-zirconia composites with calcium fluride additions. *J. Am. Ceram. Soc.*, 2002, **85**(6), 1634–1636.
25. Kim, H. W., Noh, Y. J., Koh, Y. H., Kim, H. E. and Kim, H. M., Effect of CaF_2 on densification and properties of hydroxyapatite-zirconia composites for biomedical applications. *Biomaterials*, 2002, **23**, 4113–4121.
26. Kim, H. W., Lee, S. Y., Bae, C. J., Noh, Y. J., Kim, H. E., Kim, H. M. and Ko, J. S., Porous ZrO_2 bone scaffold coated with hydroxyapatite with fluorapatite intermediate layer. *Biomaterials*, 2003, **24**, 3277–3284.
27. Murugan, R. and Ramakrishna, S., Effect of ZrO_2 on the formation of calcium phosphte bioceramics under micrwave irradiation. *Mater. Lett.*, 2003, **58**, 230–234.
28. Kim, H. W., Kong, Y. M., Koh, Y. H. and Kim, H. E., Pressureless sintering and mechanical and biological properties of fluor–hydroxyapatite composites with zirconia. *J. Am. Ceram. Soc.*, 2003, **86**(12), 2019–2026.
29. Kumar, R., Prakash, K. H., Cheang, P. and Khor, K. A., Microstructure and mechanical properties of spark plasma sintered zirconia–hydroxyapatite nano-composite powders. *Acta Mater.*, 2005, **53**, 2327–2335.
30. Heimann, R. B. and Vu, T. A., Effect of CaO on thermal decomposition during sintering of composite hydroxyapatite-zirconia mixtures for monolithic bioceramic implants. *J. Mater. Sci. Lett.*, 1997, **16**, 437–439.
31. Balamurugan, A., Balossier, G., Kannan, S., Michel, J., Faure, J. and Rajeswari, S., Electrochemical and structural characterisation of reinforced hydroxyapatite bioceramic sol–gel coatings on surgical grade 316L SS for biomedical applications. *Ceram. Int.*, 2007, **33**, 605–614.
32. Evis, Z., Reactions in hydroxylapatite–zirconia composites. *Ceram. Int.*, 2007, **33**, 987–991.
33. Ben Ayed, F., Bouaziz, J., Sintering of tricalcium phosphate–fluorapatite composites by addition of alumina. *Ceram. Int.*, in press. http://dx.doi.org/10.1016/j.ceramint.2007.07.017.
34. Vogel, W., Holland, W., Naumann, K. and Gummel, J., Development of machineable bioactive glass-ceramics for medical uses. *J. Non-Cryst. Solids*, 1986, **80**(1–3), 34–51.
35. Capoglu, A., Elimination of discolouration in reformulated bone China bodies. *J. Eur. Ceram. Soc.*, 2005, **25**, 3157–3164.
36. Lee, W. E. and Rainforth, W. M., *Ceramic Microstructure: Property Control by Processing*. Chapman & Hall, 1994.
37. Brunauer, S., Emmet, P. H. and Teller, J., Adsorption of gases in multimolecular layers. *J. Am. Chem. Soc.*, 1938, **60**, 310–319.
38. Yashima, M., Sakai, A., Kamiyama, T. and Hoshikawa, A., Crystal structure analysis of β-tricalcium phosphate $Ca_3(PO_4)_2$ by neutron powder diffraction. *J. Solid State Chem.*, 2003, **175**, 272–277.
39. Celaletdin, E., Webster, T. J., Bizios, R. and Doremus, R. H., Hydroxylapatite with substituted magnesium, zinc, cadmium, and yttrium: Structure and microstructure. *J. Biomed. Mater. Res.*, 2001, **59**(2), 305–311.